Tellus (1989), *41B*, 256–271

Simulated global distribution and deposition of reactive nitrogen emitted by fossil fuel combustion

By HIRAM LEVY II and WALTER J. MOXIM, *Geophysical Fluid Dynamics Laboratory/NOAA, Princeton University, P.O. Box 308, Princeton, NJ 08542, USA*

(Manuscript received 12 April 1988; in final form 11 October 1988)

ABSTRACT

We use the medium resolution (~265 km horizontal grid) GFDL general circulation transport model to simulate the global spread and deposition of reactive nitrogen emitted by fossil fuel combustion. The nitrogen species are transported as a single tracer with no explicit chemistry. Chemical reactions are only present implicitly in the bulk coefficients for dry and wet removal. The observed wet deposition of nitrogen over North America is used to determine the global parameter for wet deposition, and constant bulk coefficients for dry deposition over land and sea are pre-calculated from measured concentrations and deposition velocities. The simulated yearly depositions in Western Europe and at regional export sites, as well as simulated yearly concentrations and their seasonal variation over the North Pacific, are compared with available observations. The agreement is generally quite good and almost always within a factor of 2. This model is then used to identify a number of important source regions and long-range transport mechanisms: (1) Asian emissions supply two-thirds of the soluble nitrogen compounds over the North Pacific. In the summer, North American emissions are important over the subtropical North Pacific. (2) Nitrogen emissions from Europe dominate the nitrogen component of Arctic haze in the lower troposphere, while North American and Asian emissions are only important locally. The model predicts a large gradient in the Arctic with average winter mixing ratios ranging from less than 0.1 ppbv over Alaska to more than 1 ppbv over eastern Russia. (3) Throughout the Southern Hemisphere, the emissions from fossil fuel combustion account for 10% or less of the observed soluble nitrogen at remote sites, an amount less than a previously simulated contribution from stratospheric injection. The long-range transport of PAN, NO_y production by lightning and biomass burning, and some, as yet, unknown marine biogenic source may all supply part of this background soluble nitrogen. However, the similarity between the seasonal cycles observed at Samoa for soluble nitrogen and for O_3, a species known to be supplied from the stratosphere, suggests a major rôle for either stratospheric injection or an upper tropospheric source.

1. Introduction

Reactive nitrogen compounds play a major rôle in the atmospheric chemistry of the troposphere over a wide range of spatial scales and environmental issues. The impact of nitrogen oxides on photochemical smog, a local phenomenon, has been well documented (e.g., Leighton, 1961), and the regional problem of acid rain, of which acidic nitrogen is one of the two principal components, has also been widely discussed (e.g., NRC, 1983). Through their impact on the level of tropospheric O_3 (Crutzen, 1974) and OH (Levy, 1971), nitrogen oxides play a major rôle in the global reactivity of the troposphere. This reactivity, in turn, controls the level of a number of greenhouse gases that influence the environment on a global scale. At this time there is insufficient observational data to determine the global distribution of reactive nitrogen. This global simulation provides a first look at such distributions.

The largest source of reactive nitrogen in the global nitrogen cycle, the combustion of fossil

fuels, results in an estimated yearly global source of 21×10^{12} grams of nitrogen (21 tg N) (Logan, 1983). This surface source greatly exceeds the other documented global source, stratospheric injection, which has a range of 0.5–1.0 tg N (Levy et al., 1980). While a number of other sources have been suggested, (lightning, biomass burning, microbial activity) estimates of their global contribution are quite uncertain and none are currently thought to be as important as fossil fuel combustion (e.g., Logan, 1983).

In this study a medium resolution ($\sim$265 km grid) general circulation transport model (Mahlman and Moxim, 1978) is used to simulate the global climatology of reactive nitrogen resulting from fossil fuel combustion. The parent general circulation model (Manabe et al., 1974) generates an ensemble of realistic weather patterns that compares well with observed yearly climatology and with observed meteorology on time scales ranging from six hour synoptic events to seasonal cycles. While regional forecast models may generate more realistic simulations of individual synoptic events and provide valuable insights to specific transport processes and deposition events (e.g., Chang et al., 1987), these models have not yet generated climatologies of concentration and deposition. Such data is needed for studying both the cumulative impact of acid deposition on a regional environment and the global nitrogen budget.

First, we simulate the distribution and deposition of the global emissions of combustion nitrogen and compare the model's results with available observations. Major sources of nitrogen in remote regions are then identified and conclusions are drawn regarding the impact of combustion NO_x on the Southern Hemisphere, the possible impact of peroxyacetylnitrate (PAN) on global-scale transport and the potential rôle for other less certain sources of reactive nitrogen.

2. Model description

The GFDL general circulation/transport model has 11 terrain following levels with standard heights of 31.4, 22.3, 18.8, 15.5, 12.0, 8.7, 5.5, 3.1, 1.5, 0.5, 0.08 km and a horizontal grid size of approximately 265 km or 2.4°. The off-line transport model has a time step of $\sim$26 min and is driven by 6-h time-average winds and precipitation that are generated for one year by the parent general circulation model. This parent GCM has no diurnal variation of insolation and will not realistically simulate atmospheric fluctuations with periods shorter than 6 h. However, it has been very successful in simulating many features of the earth's climate (Manabe et al., 1974; Manabe and Holloway, 1975), and resolves weather events such as frontal passages, anticyclones, and mid-latitude cyclones. The transport model is integrated for 17 months for each source scenario and the last 12 months are used for this study.

2.1. Transport

For this study, NO_y represents the sum of all gaseous and particulate nitrogen compounds, with the exception of N_2O, resulting from both direct emission and chemical transformations. This collection of reactive nitrogen compounds is transported as a single tracer that satisfies the following continuity equation:

$$\frac{\partial R p_*}{\partial t} = -\nabla_\sigma \cdot V_2 p_* R - \frac{\partial}{\partial \sigma} \dot{\sigma} p_* R + \text{diffusion} + \text{source} - w_{\text{eff}} p_* R_{\text{surf}} - \Phi p_* R. \quad (1)$$

R is the NO_y volume mixing ratio, p_* is surface pressure, V_2 is the horizontal wind, $\sigma = p/p_*$ is the vertical coordinate where p is pressure, w_{eff} is the group deposition velocity that is 0.0 in all but the lowest level, R_{surf} is the NO_y volume mixing ratio at the surface and Φ is the group precipitation removal coefficient. The preparation of input data, numerical integration techniques and model characteristics have all been described in previous simulations of tropospheric nitrous oxide and ozone and the distribution and deposition of nuclear debris (Mahlman and Moxim, 1978; Levy et al., 1982; Levy et al., 1985).

"Diffusion" includes both explicitly parameterized horizontal and vertical subgrid-scale diffusion and an implicit contribution from the computational adjustment of negative mixing ratios (Mahlman and Moxim, 1978). The standard vertical diffusion term, which dominates vertical transport in the lower troposphere when the model is convectively unstable (dry or moist) on the grid scale, has been described previously (Levy et al., 1982). However, to account for turbulent mixing in the boundary layer when the

model is stable on the grid scale, we include an additional shear-dependent vertical diffusion term

$$k_v = A\,L(z)^2 |\partial V/\partial z|,$$

where $L(z)$ is 27 m, 17 m and 0.75 m in the bottom three levels respectively and 0.0 above. $A = 0.1$ gives the best agreement between mid-continental winter profiles for ^{222}Rn simulated by this transport model and profiles based on an analysis of available observations (Liu et al., 1984).

2.2. *Source*

The global source function in eq. (1), "source", is constructed from a variety of emission inventories, fuel use statistics and emission factors, and is held constant in time for each grid box. There is no seasonal cycle in the source, and neither the parent GCM, the off-line transport model nor the source has a diurnal cycle. While Europe, because of low demand for cooling in the summer and high demand for heating in the winter, is believed to have a seasonal cycle in NO_x emissions, it is less than the uncertainty in the absolute source strength and not important to this study.

The US and Canadian portion of the global source is constructed from EPA and Environment Canada emission inventories, and has been described previously (Levy and Moxim, 1987). The area emissions are released at the model's surface, and the point sources are apportioned, according to stack height, among the surface and mid-points of the bottom two levels. Of the resulting total yearly emissions (7.5 tg N), 65% are injected at the surface, 20% into the middle of the lowest level at a standard height of 80 m, and 15% are injected into the middle of the next level at a standard height of 500 m. While emissions at both the surface and 80 m enter the same level, the surface emissions experience an immediate reduction due to dry deposition (see Subsection 2.4 for more detail).

The NO_x emissions for Europe are compiled by EMEP (Eliassen et al., 1988). We release the area sources at the surface and split the point sources evenly between the bottom two levels. The resulting yearly source for Europe is 5.9 tg N with 44% released at the surface and 28% released into each of the bottom two levels.

The remainder of the global emissions (7.9 tg N) are based on a country by country compilation of UN fuel use statistics and EPA emission factors (Hameed and Dignon, 1988). A given country's emissions are then distributed among the model grid boxes by population and further apportioned among the surface and bottom two levels in the fraction 0.4, 0.4, and 0.2 respectively. The distribution of total yearly emissions at 21.3 tg N is shown in Fig. 1.

2.3. *Chemistry*

Chemical reactions indirectly control deposition by converting insoluble nitrogen compounds to soluble nitric acid and nitrate and apportioning NO_y among the various species with their differing deposition velocities. Extensive gas-phase chemical reaction schemes have been developed (e.g., Leone and Seinfeld, 1985), and a simplified version (Stockwell, 1986) has been recently employed in a regional acid deposition model (Chang et al., 1987). Though these chemical schemes can reproduce smog chamber experiments, they have only recently been compared with the chemistry in the background continental troposphere (e.g., Trainer et al., 1987).

The detailed chemistry is most important within the source region. NO_y is transported relatively slowly in the boundary layer (100–200 km/day) and generally lost to dry deposition in 1–2 days, regardless of the chemical partitioning. Once in the free troposphere, a region not directly affected by boundary layer processes, removal is less likely and chemical partitioning is again less important. Chemical partitioning may, however, play an important rôle in the wintertime Arctic where PAN is the dominant form of NO_y (Bottenheim et al., 1986) and the collective tracer model underestimates both the effective NO_y lifetime and its transport.

To realistically simulate the impact of fossil fuel combustion on the global nitrogen budget, the model must generate the correct long-range transport of nitrogen combustion products from the major source regions. Besides a realistic meteorology, this requires that the correct fraction of combustion nitrogen be available for transport, after dry and wet removal in the source region. Rather than using a complex chemical reaction scheme to generate HNO_3 formation rates and surface partitionings that reproduce

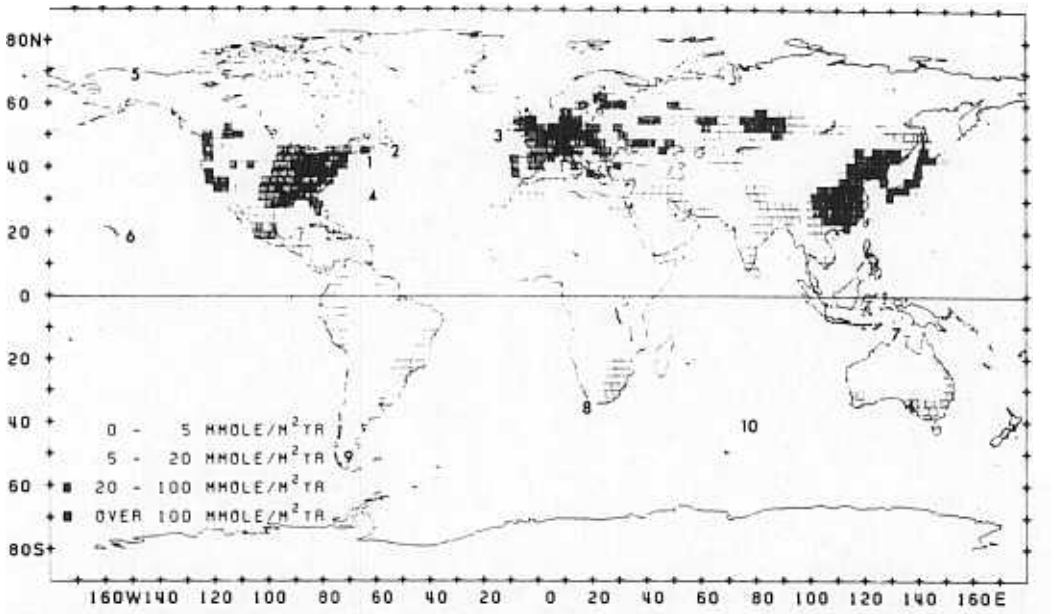

Fig. 1. Yearly total combustion nitrogen emissions (mMole m^{-2} yr^{-1}) for the globe with remote wet deposition sites (1–10) identified.

observed depositions, we transport the reactive nitrogen species collectively as NO_y and base the model's parameterizations for wet and dry removal on observations of deposition and surface concentration from the North American source region (Levy and Moxim, 1987). The global applicability of this parameterization is discussed in Subsection 3.2.

2.4. *Dry deposition*

The loss of gases and particles by their sticking to or reacting with the earth's surface and its vegetation as well as their absorption by that same vegetation is a *continuous* process called dry deposition. This process depends on the local mixing ratio of the individual reactive nitrogen species at the surface, $R_{surf}(i)$, and on their respective deposition velocities, $w_0(i)$. In the model, the nitrogen species are transported collectively as $R(NO_y)$ and dry deposition is a product of two quantities:

(1) An effective or group deposition velocity that depends on the chemical partitioning of NO_y,

$$w_{eff} = \frac{}{R_{surf}(NO_y)} \sum_i R_{surf}(i)\, w_i, \qquad (2)$$

where $R_{surf}(i)$ is the volume mixing ratio of the ith reactive nitrogen species at the surface and w_i is its measured deposition velocity.

(2) The mixing ratio of the collection of reactive nitrogen species at the surface.

By assuming that the bottom half of the lowest level is in steady state with surface deposition balanced by turbulent flux, we can write

$$R_{surf} = R_{ll}/[1 + (w_{eff}/C_d|V_{eff}|)], \qquad (3)$$

where C_d is the GCM's globally averaged surface drag coefficient (0.002), R_{ll} is the mixing ratio in the lowest level and $|V_{eff}|$ is the model's effective surface wind speed. For more details on eq. (3), see Levy et al. (1985). For a recent discussion of dry deposition in general, see Walcek et al. (1986).

Measurements of w_i over land are available for NO_2 (0.3–0.4 cm s^{-1}); PAN (0.3–0.4 cm s^{-1}); HNO_3 (1.0–2.5 cm s^{-1}) (Cadle et al., 1985; Huebert and Robert, 1985; Wesely et al., 1982; Garland and Penkett, 1976; Walcek et al., 1986; Voldner et al., 1986). Only HNO_3 is assumed to be deposited over snow and water, and w_i is assumed to be 0.0 everywhere for NO. Using these values and the seasonal average partitioning of NO_y based on limited measurements near

Boulder, CO; Point Arenas, CA; and State College, Pa (Fahey et al., 1986; Fehsenfeld et al., 1988), we calculate w_{eff} over snow-free land ranging from 0.30 cm s^{-1} in the winter to 0.50 cm s^{-1} in the summer. Using data compiled by Logan (1983), we calculate, outside of urban areas, w_{eff} ranging from 0.6 to 0.25 cm s^{-1}. While both the chemical partitioning and the individual deposition velocities exhibit considerable variability in both space and time, the seasonal average of w_{eff} remains bounded over a relatively narrow range.

We use $w_{eff} = 0.3$ cm s^{-1} over land and 0.1 cm s^{-1} over sea as constant deposition coefficients for the collection of reactive nitrogen species comprising NO_y. This neglects both spatial variability due to difference in ground cover and seasonal effects due to changes in temperature, snow cover and chemical partitioning. Such a simplification is most serious in the winter high latitudes where even HNO_3 is weakly removed (Johansson and Granat, 1986).

To determine the model's sensitivity to w_{eff}, separate simulations with the North American source were performed for an upper and lower limit of w_{eff} over land, 1.0 and 0.1 cm s^{-1} (Levy and Moxim, 1987), and for an upper limit of w_{eff} over ocean, 0.5 cm s^{-1}. Using $w_{eff} = 1.0$ over land, a value appropriate to $HNO_3 = NO_y$, led to a very rapid loss by dry deposition over the source regions and resulted in surface concentrations and wet deposition over export locations that were much smaller than observed. The lower limit over land, a value appropriate to snow covered ground with HNO_3 no more than $0.1\,NO_y$, produced surface concentrations in the North American source region that were too high. To estimate the impact of NO_y aging, w_{eff} over the ocean was increased to 0.5 cm s^{-1} during the summer months. Even for the subtropical North Pacific where long-range transport occurs in the lower, albeit stable, troposphere just above the maritime boundary layer, NO_y was reduced by only 20%. The neglect of NO_y aging should not qualitatively affect our conclusions regarding the impact of combustion emissions on the nitrogen budget in the remote maritime atmosphere.

An additional source of dry deposition in the model is the immediate deposition of a fraction of the emissions released at the surface of the model's lowest level. This is a result of the mathematical solution for surface deposition in the presence of a surface source and produces a 7% reduction in the total emissions. Though small relative to the uncertainties in the absolute source strength, it does make a significant contribution to dry deposition in the source region.

2.5. *Wet deposition*

Precipitation removal, an *intermittent* process acting throughout the tropospheric column, is also expressed as a first order loss term in eq. (1). The removal coefficient at level k, Φ_k, is given by

$$\Phi_k = N B_k[\text{rain}/\text{rain}^G] \tag{4}$$

where "rain" is the model's accumulated 6-h precipitation in a given column, "rain^G" is the global average precipitation rate expressed as deposition per 6 h, $1/B_k$ is a lifetime that, based on observations of the vertical distribution of rainfall production, ranges from 20 days at the lowest level to 60 days at the 8.7 km level (Mahlman and Moxim, 1978), and N is a global empirical parameter. A much more complex formulation based on Henry's Law solubility and a cloud physics parameterization including rainout in the cloud and washout below reduces to a form similar to eq. (4) for highly soluble gases (private communication, W. L. Chameides). The wet deposition of radioactive debris from nuclear tests in the stratosphere has been successfully simulated with $N = 1$ (Mahlman and Moxim, 1978).

For this and a previous study of nitrogen emissions (Levy and Moxim, 1987), the empirical parameter is adjusted to $N = 9$ to bring the simulated yearly integral of nitrogen deposition in precipitation over the US and Canada into agreement with the observed deposition of ~ 2 tg N (Logan, 1983; Golomb, 1983; Barrie and Hales, 1984; Galloway and Whelpdale, 1987). North America was chosen because it has the most complete data and is least affected by outside sources. We include no seasonal dependence in Φ_k, in agreement with recent analysis (Summers and Barrie, 1986). While the yearly integral has been adjusted, the spatial pattern and seasonal variation has not been fixed. It depends on the model's wind fields and precipitation patterns and is in good agreement with observations (Levy and Moxim, 1987). While we might not expect $N = 9$ to apply throughout the world,

there are sufficient deposition data to confirm the applicability of $N = 9$ for the Northern Hemisphere. This will be discussed in Subsection 3.2 on model evaluation.

For a quick qualitative check on our choice of N, we consider an extremely simplified model of a mid-latitude precipitation event and calculate the resulting deposition using both eq. (4) and the oxidation of NO_2 to HNO_3 by OH. Specifying rain = 3 cm day^{-1} for 12 h, we assume transport only in the vertical. With a velocity of 10 cm s^{-1}, a volume of air will rise from the surface to 4.32 km during the 12-h event.

The HNO_3 formation during the storm depends on the fraction of NO_y existing as HNO_3 when the precipitation starts and the rate at which NO_2 can be converted to HNO_3 during the event. The chemical calculations use daily average OH profiles ranging from 1.2×10^6 molecules cm^{-3} at the surface to 0.4×10^6 molecules cm^{-3} at 6 km for the winter and 3.5×10^6 to 1.8×10^6 molecules cm^{-3} for the summer (Levy, 1974). OH is further reduced by 0.5 to account for the affect of clouds on O^1D production, and the initial partitioning of NO_y is the same as that used for the calculations of w_{eff}. Over the 12-h period of the storm, the chemical calculations find that, while being lifted, 25% of the surface NO_y is converted to HNO_3 and removed in the winter and 40% in the summer to give an average of 32.5%. Over the same period, the precipitation parameterization gives an average NO_y removal in the rising parcel of 13% for $N = 1$ and 71% for $N = 9$. This qualitative agreement supports the simple first-order treatment of wet removal.

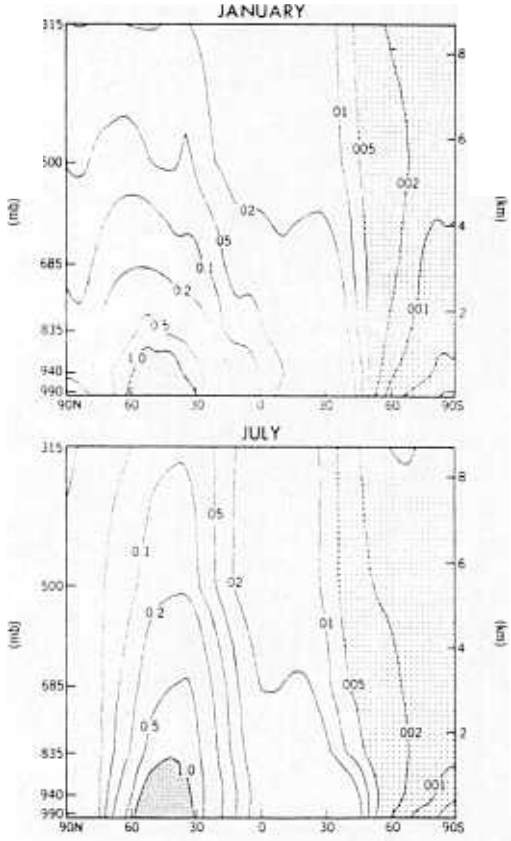

Fig. 2. Latitude–height plots of $R(NO_y)$ (ppbv) averaged over longitude for the months of January and July.

3. The global distribution and deposition of combustion nitrogen

After examining the simulated distribution and deposition of global combustion nitrogen emissions, the model's results are compared with the observed yearly depositions in Europe, nearby export sites and remote locations, and with the yearly concentrations at background sites in the North Pacific. Then, the global model is used to determine the impact of combustion emissions on NO_y levels in the Arctic, the North Pacific and the Southern Hemisphere and to identify the source regions responsible for each.

3.1. Model simulations

Just as was simulated (Levy and Moxim, 1987) and calculated from observation (Galloway and Whelpdale, 1987) for North America, acid rain over the world's source regions accounts for a small portion (30%) of the global combustion emissions of nitrogen, while dry deposition over the source regions accounts for 45% and export, mainly over the oceans, for the remaining 25%.

Latitude–height plots of NO_y, averaged over longitude for a month, are shown in Fig. 2 for both January and July. Previously we observed that less than 0.1% of the North American emissions are transported to the Southern Hemisphere (Levy and Moxim, 1987) and this appears to hold true for the global source where the Southern Hemisphere NO_y levels seldom ex-

ceed 0.05 ppbv. Unlike insoluble tracers dominated by Northern Hemisphere surface sources (Prather et al., 1987; Plumb and Mahlman, 1987), there is no zonally averaged inversion in the southern hemisphere. Transport through the ITCZ rainbelt effectively removes most of the NO_y before it can be carried up into the middle troposphere. The strongest seasonal pattern occurs in the northern hemisphere where most of the emissions occur. In the winter the 100 pptv contour spreads to 90°N though not above 500 mb. In the summer, strong convective mixing over the continental source regions lifts this contour to 315 mb at mid-latitudes, but there is little transport north of 75°. The small stratospheric source of NO_y, predicted to support zonal averages of 0.01–0.03 ppbv in the boundary layer and 0.03–0.05 ppbv in the free troposphere (Levy et al., 1980), appears to be more important than fossil fuel combustion over most of the Southern Hemisphere and the upper troposphere of the Northern Hemisphere. Unlike emissions at the ground that generally undergo wet removal when they are lifted into the free troposphere for long-range transport, NO_y from the stratosphere or upper troposphere is transported in dry and relatively stable air. There is also a possible rôle for nitrogen emissions from biomass burning in the tropics (Crutzen et al., 1985), although the NO_y must survive wet removal processes when it is lifted into the upper troposphere before being transported to higher latitudes.

The simulated NO_y distributions also have large longitudinal gradients, as are shown by latitude–longitude plots of yearly averaged NO_y mixing ratio in the boundary layer (990 mb) and the middle troposphere (500 mb) along with the plot of total yearly wet deposition (see Fig. 3). As expected for a short-lived tracer, there is a strong relationship between the distributions in Fig. 3 and the source distribution in Fig. 1. In all cases the maxima occur near the source regions, though at 500 mb the gradients are much weaker and NO_y is carried down wind. Throughout the troposphere, the NO_y mixing ratio is low (0.05 ppbv or less) over the North Pacific and less than 0.005 ppbv (see the dotted contour in Fig. 3) over much of the southern ocean. The only significant seasonal differences in the fields shown in Fig. 3 are a summertime increase in vertical transport due to increased continental convection, an increased downwind transport at mid-latitudes in the winter when the prevailing westerlies are strongest (particularly over the North Pacific), and increased summertime easterly transport in the tropics and subtropics.

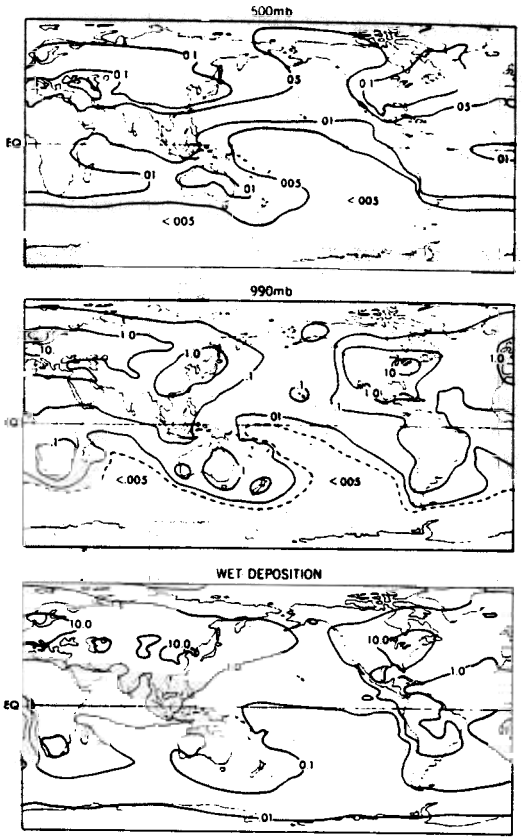

Fig. 3. Latitude–longitude plots of the yearly averages of $R(NO_y)$ (ppbv) at 500 mb in the free troposphere and 990 mb in the surface layer and of the yearly total wet deposition of nitrogen (mMole m^{-2} yr^{-1}).

While there is no inversion in the zonal mean profiles (Fig. 2), significant regional inversions do occur in both hemispheres over the central Atlantic and Pacific which are down wind of, but distant from, major source regions (Fig. 4). Most of the long-range transport in the atmosphere, as simulated in Fig. 4 and inferred from trajectory studies in the real atmosphere (Merrill et al., 1985), occurs in the free troposphere not in the boundary layer.

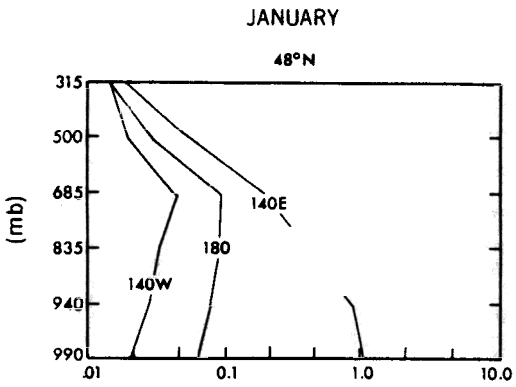

Fig. 4. Local vertical profiles of monthly averaged $R(NO_y)$ (ppbv) simulated for 3 sites at 48°N latitude (Japan (140°E), Central Pacific (180°), Eastern Pacific (140°W)) in January.

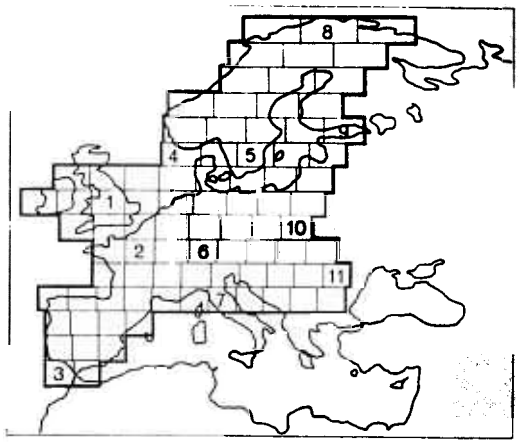

Fig. 5. Map of the European source region with the model grid superimposed, with the grid boxes containing the wet deposition sites from Table 1 identified, and with the integrated wet deposition region outlined.

3.2. *Model evaluation*

While model results have intrinsic value, the key issue is the model's ability to simulate the behavior of the real atmosphere and, in this case, real atmospheric transport. To establish this, we compare the model's simulations with available observations.

The wet removal parameter ($N = 9$) and the calculated values for w_{eff}, 0.3 cm s^{-1} over land and 0.1 cm s^{-1} over ocean, are based on observations in North America. First we check their global applicability. The observed yearly deposition over the region of Europe outlined in Fig. 5, 1.6 tg/yr (Schaug et al., 1987), compares well with the model's self-determined value of 1.4 tg/yr. A more detailed comparison is provided in Table 1 where yearly wet deposition and precipitation are compared for a number of representative stations whose locations are noted in Fig. 5. The agreement is generally within 25% and seldom worse than a factor of 2. The largest disagreements between model and observations occur in regions with sharp topographical gradients that produce precipitation features not resolved by the model (i.e., Station 4). As noted by the reviewer, the model, while frequently simulating higher precipitation than observed over Europe, almost always simulates lower wet deposition. It appears that the model's parameterization underestimates wet deposition in Europe by 15%–20%. While yearly deposition data from the third major source region, Asia, are not available, the comparison in Europe is encouraging. Our very simple parameterization appears to simulate realistic deposition in source regions and, as a result, should provide a realistic effective source for long-range transport.

Table *Nitrogen wet deposition at European sites*

Station no.	Precip. (cm yr^{-1})		Wet dep. (mMole m^{-2} yr^{-1})	
			obs.	model
1	52	86	22	29
2	71	89	36	23
3	30	44	3	3
4	180	70	46	
5	50	68	19	13
6	161	127	46	45
7	57	88	22	16
8	38	61	3	3
9	49	67	16	13
10	54	97	30	25
11	57	87	13	15

In Table 2, the model's wet deposition values are compared with observations (J. N. Galloway, private communication) from regional stations no more than 1000–2000 km downwind of major sources (Adrigole, Ireland; Bermuda; Bay DeSpoir, Newfoundland; Katherine, Australia; Nova Scotia) and from remote locations only

Table 2. *Nitrogen wet deposition at regional and remote sites*

Station name	No.	Precip. (cm yr^{-1})		Wet dep. (mMole m^{-2} yr^{-1})	
		obs.	model	obs.	model
Nova Scotia	1	138	116	16.0	15.0
Bay de Espoir, Nfld.	2	149	93	9.1	10.0
Adrigole, Ireland	3	200	90	11.2	5.3
Bermuda	4	140	189	6.3	5.4
Poker Flats, Alaska	5	29	30–50*	0.5	0.2–0.7*
Mauna Loa, Hawaii	6	47	97	0.5	0.3
Katherine, Australia	7	91	33–99*	4.0	0.1–0.2*
Cape Point, SA	8	36	20	1.6	0.2
Torre de Paine, Chile	9	49	135	0.2	0.1
Amsterdam, Island	10	123	138	1.9	0.1

* Because of a steep gradient in model precipitation, neighboring boxes were included.

affected by long-range transport (Amsterdam Island; Torre del Paine, Chile; Poker Flat, Alaska; Mauna Loa, Hawaii; Cape Point, South Africa). These sites are located on Fig. 1. With the exception of Amsterdam Island, all the remote sites have local topography that the GCM cannot resolve, and Katherine, Australia, though receiving 91 cm yr^{-1} of rain, is only a few hundred kilometers from the desert. As a further difficulty, only a fraction of the yearly deposition is collected and analyzed at the remote sites, and we find that deposition, at sites strongly influenced by the transport of NO_y, is not linear in precipitation.

Model and observation are in excellent agreement for 3 of the regional deposition sites. Most of the disagreement at Adrigole is due to the difference in local precipitation, not due to errors in the regional and long-range transport. However, even when the deposition from background nitrogen is subtracted from the Katherine, Australia data and the error in simulated precipitation is considered, model and observation are far apart. The local combustion source, see Fig. 1, is weak with no large sources nearby. Unless a major industrial source has been missed, the most likely explanation is a large agricultural source which is not part of this study. The agreement at 4 of the 5 regional sites and the two remote sites in the Northern Hemisphere is within a factor of 2 or better. The model's low values may be due to its lack of explicit transport of insoluble end-products such as PAN and/or to its highly simplified parameterization of wet deposition.

In Table 3 we compare mixing ratios from the model's lowest level with observations (Prospero et al., 1985; Savoie et al., 1988) from a string of island stations running from Shemya in the North Pacific to Norfolk Island in the South Pacific (see Fig. 6). The filter measurements are lower limits since water insoluble species, mainly organic nitrates and nitrogen oxides are not included. While some surface measurements of the

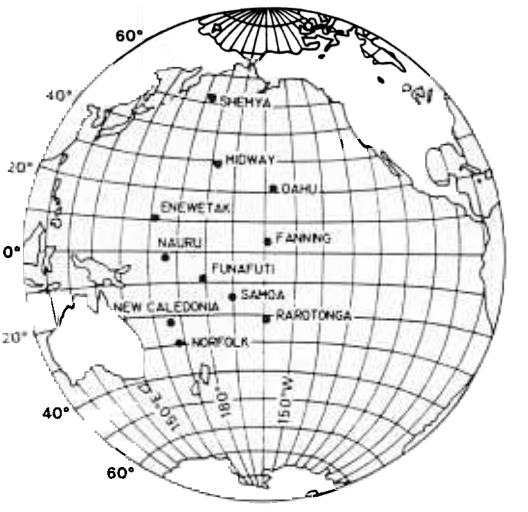

Fig. 6. Map showing the approximate location of the Pacific network of surface stations measuring total water-soluble NO_y.

Table 3. *Surface* $\overline{R(NO_y)}^{yr}$ *(ppbv) in the Pacific*

Station	Obs.	Obs. – Background (0.038 ppbv)	Model
Shemya	0.094	0.056	0.074
Midway	0.105	0.067	0.043
Oahu, Hawaii	0.130	0.092	0.033* (0.050–0.060)†
Enewetak	0.054	0.016	0.020
Fanning	0.058	0.020	0.011
Nauru	0.058	0.020	0.004
Funafu'ti	0.040	0.002	0.003
Samoa	0.043	0.005	0.003
Rarotonga	0.042	0.004	0.004
New Caledonia	0.076	0.038	0.010–0.050†
Norfolk	0.065	0.027	0.028

* The local Hawaiian source has been eliminated in this simulation.

† Because of the presence of a local source, data has been taken from upwind boxes.

insoluble species over the eastern North Pacific have been as high as 0.03–0.05 ppbv (Singh et al., 1986; Atlas, 1988), NO_x in the central Pacific is much lower (e.g., McFarland et al., 1979) and PAN is at the measurement limit of ~0.005 ppbv over the South Pacific (Singh et al., 1986). Therefore, the insoluble nitrogen species are not expected to make a major contribution to the surface measurements of NO_y over the Central Pacific. As was the case for deposition in maritime locations, the surface measurements are corrected for the background soluble nitrogen (0.038 ppbv) measured at extremely remote maritime sites (Savoie et al., 1988).

With the exception of Nauru, model and observation agree within a factor of 2. A more serious difference is the latitude gradient in the Northern Hemisphere. While the model lacks explicit transport of PAN and a time-dependent w_{eff}, the Shemya observations are uncertain because of a limited record (Prospero et al., 1985) and those at Oahu, though only taken from on-shore winds, are made in a region of relatively high emissions. At this time it is not clear which latitude-gradient is correct. However, measured surface concentrations of Asian dust increase with latitude (Uematsu et al., 1985), just as we simulated for Asian emissions of NO_y.

Although there are clearly quantitative errors in the model's simulation of long-range transport and deposition, the degree of agreement, given the lack of explicit chemistry and the simple parameterizations of deposition, is reassuring.

3.3. The nitrogen component of arctic haze

Arctic haze was first reported in the scientific literature by Mitchell (1956). Following the demonstration of its association with mid-latitude combustion by Rahn et al. (1977), there has been a great deal of research (see Barrie (1986)). In the wintertime Arctic, which has a very stable boundary layer, little precipitation, a low temperature and a snow or ice covered surface, HNO_3 and NO_3^- are deposited slowly (Johansson and Granat, 1986), and PAN, NO and NO_2 all have very long lifetimes. With the European source region, shown in Fig. 1, almost 20° north of its counterpart in North America and with significant European emissions inside the Arctic Circle, one might expect the European emissions to be the major cause of Arctic haze. Model simulations (e.g., Barrie et al., 1989) find this to be true for sulfate, though the relative importance of emissions north and south of the Arctic Circle is still an issue.

In Fig. 7, the average winter NO_y mixing ratios in the boundary layer are presented for 4 source scenarios: (1) global emissions; (2) North American emissions; (3) Asian emissions; (4) emissions north of 60° N. For this seasonal study, the simulations begin in October and are integrated through March. In general European emissions dominate, though North American and Asian emissions are important in their local Arctic regions. Emissions north of 60° N contribute up to half of the NO_y in the European Arctic. Further detail is given in Table 4. We see

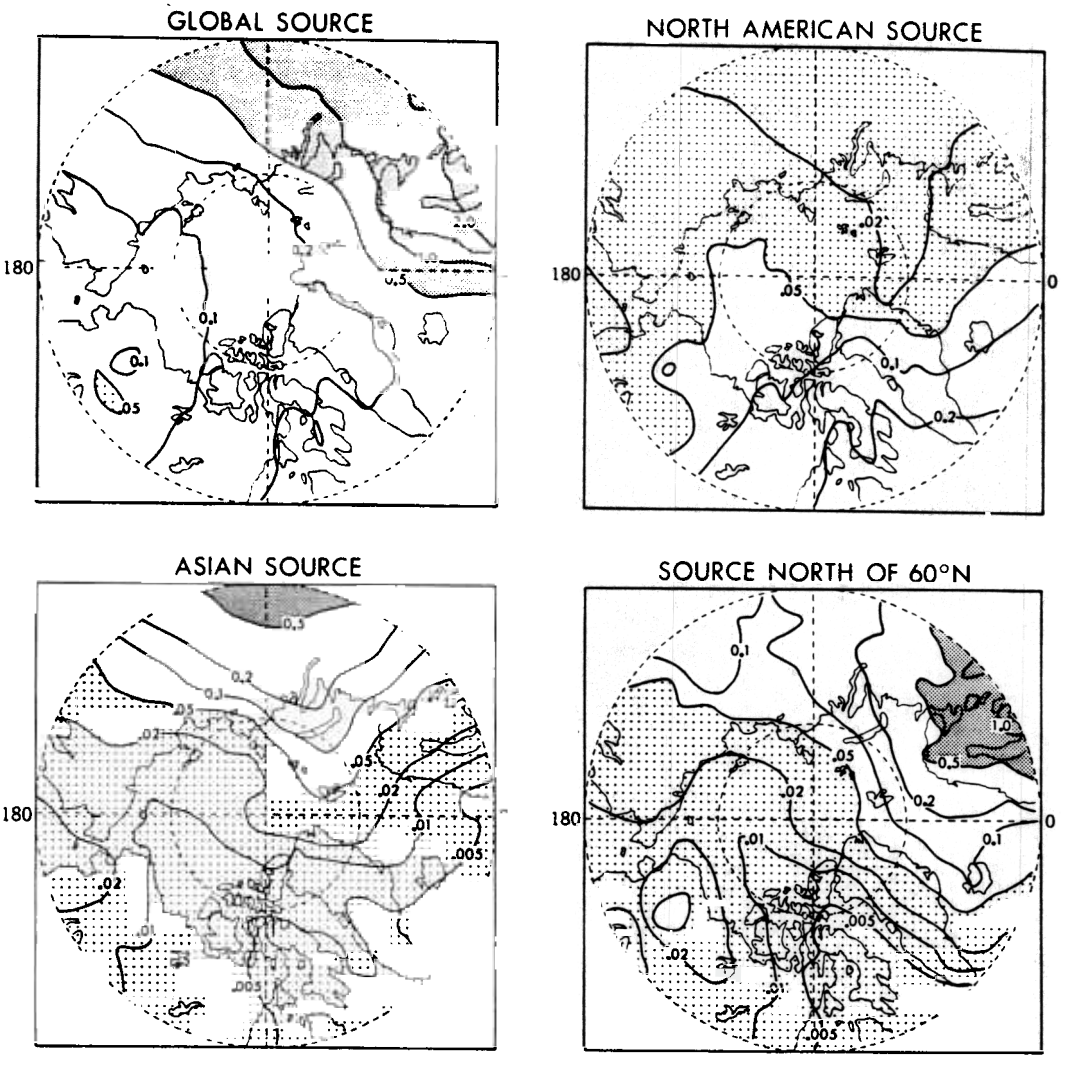

Fig. 7. Polar stereographic plots of the winter (Jan.–Feb.–Mar.) average $R(NO_y)$ (ppbv) at 940 mb (standard height of 500 m) for 4 sources: global emissions; North American emissions; Asian emissions; global emissions north of 60°N.

that emissions inside the Arctic are responsible for half of the total NO_y at the surface, while both European and North American emissions play important rôles at higher levels. Transport to these levels in the Arctic is the result of winter extratropical cyclones that generally form over the northern US and Canada, the North Atlantic and northern Europe. The general pattern shown in Table 4 for the NO_y component of Arctic haze is in harmony with previous simulations for sulfur (e.g., Barrie et al., 1989).

The transport model predicts a strong longitudinal gradient in the NO_y with mixing ratios lower than 0.1 ppbv in northern Alaska and greater than 1 ppbv in northern Scandinavia and the Soviet Union (see Fig. 7). This pattern is qualitatively similar to the one reported by Barrie (1986) for sulfate. Whether the weaker sulfate gradient is due to quantitative differences in the emission patterns, differences in the wintertime oxidation rates, defects in the model's transport or the larger w_{eff} for NO_y is not clear. The slower

Table 4. *The % contribution to NO_y in the Arctic by source region*

Source	$R_{990\,mb}$ (%)	$R_{940\,mb}$ (%)	$R_{835\,mb}$ (%)	$R_{685\,mb}$ (%)
Global	100	100	100	100
Europe	30	44	50	46
North of 60° N	49	25	10	6
North America	10	15	26	37
Asia	11	16	14	11

oxidation rate expected for SO_2 would allow more zonal mixing of the sulfur species, while NO_y's higher w_{eff} decreases its atmospheric lifetime and understates the degree of zonal mixing.

The measurements of NO_y in the Arctic are quite limited. Bottenheim and Gallent (1986) report 0.25–0.35 ppbv NO_y at Alert in late winter, most of which is PAN and is expected to have a long atmospheric lifetime in the winter Arctic, while the model only gives 0.15–0.20 ppbv of NO_y. When w_{eff} was set to 0.0 in the Arctic, the simulated levels of NO_y exceeded the observations of Bottenheim and Gallent (1986). The model's apparent overestimation of dry deposition in the winter Arctic and its lack of explicit transport for PAN exaggerates the gradient between North America and Europe and underestimates the total amount present. However, the qualitative pattern of distribution and the dominance of the European sources is not affected. Currently, a multiple-species model, with explicit transport of PAN and a variable w_{eff}, is being developed to study the nitrogen component of Arctic haze in detail.

3.4. *NO_y over the North Pacific*

The simulated yearly average NO_y levels at the 5 surface sites in the North Pacific (see Fig. 6) have already been compared with observations in Table 3 and discussed in Subsection 3.2. The simulated and observed seasonal cycles are compared in Fig. 8 by plotting the ratio of the monthly mean to the yearly mean. The observed seasonal cycles are based on 2–7 years of observations (Savoie et al., 1988). While the maxima and minima may be shifted by a month, the basic patterns are well simulated. In general, the model does show a larger winter/spring maximum than is observed.

By turning off separate source regions we find

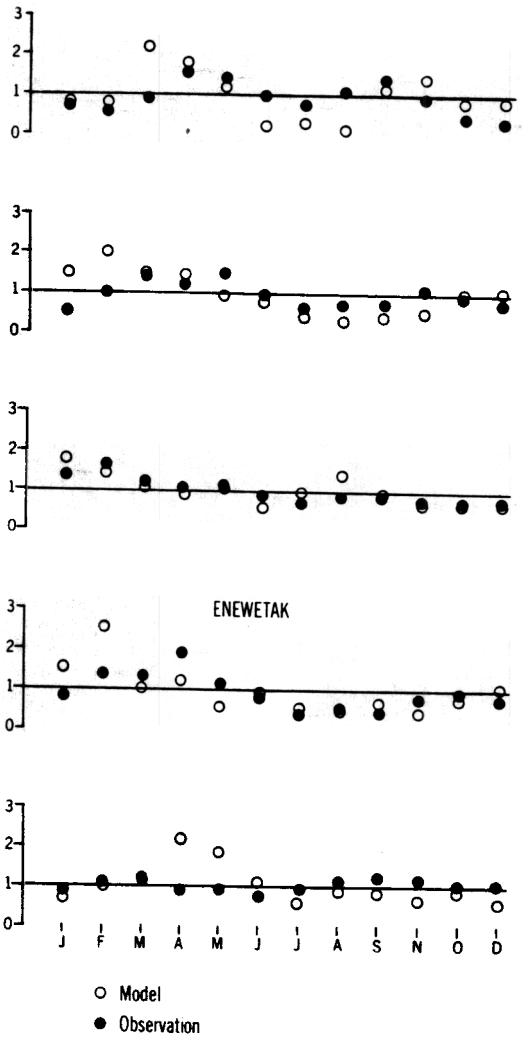

Fig. 8. Comparisons of simulated and oberved seasonal variations of surface NO_y at 5 stations in the North Pacific as given by plots of $\overline{R(NO_y)}^{mn}/\overline{R(NO_y)}^{yr}$. The open circles are the model's values and the filled circles are observations.

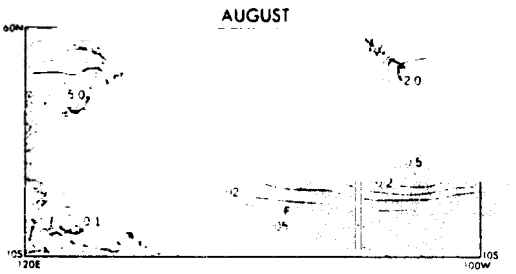

Fig. 9. Latitude–longitude plot of the average August mixing ratio for NO_y in the surface layer over the Pacific Ocean, $\overline{R_{990\,mb}(NO_y)}^{mn}$ (ppbv), as simulated by the transport model with a global source (F identifies Fanning and M identifies Midway).

that Asian emissions supply two-thirds of the NO_y over the North Pacific. The winter/spring maximum has also been observed at all 5 sites for dust transported from Asia (Uematsu et al., 1983). The second maxima at Oahu and Fanning are due to summertime transport from sources in the US. In the simulation, the summertime transport to Oahu is somewhat greater than observed, while the tongue of maximum NO_y (see Fig. 9) remains just a few hundred km north of Fanning. A southward shift of one grid box, well within interannual variability, would bring the simulation much closer to observed. High levels of NO_y have also been measured at Mauna Loa, Hawaii, in air free from contamination by either local emissions or the maritime boundary layer (Galasyn et al., 1987), and model simulations identify both springtime transport from Asia and summertime transport from the US.

3.5. *Combustion NO_y in the southern hemisphere*

Figs. 2 and 3 in Subsection 3.1 both show large interhemispheric gradients and imply that there is little interhemispheric transport of NO_y. Examining the remote Southern Hemisphere sites in Tables 2, 3, we see that the model can explain at most 10% of the observed background depositions (~ 2 mMole m^{-2} yr^{-1}) and surface concentrations (~ 0.04 ppbv) at maritime sites. The model does account for the excess NO_y at New Caledonia and Norfolk Island resulting from transported Australian emissions, though it cannot account for the observed deposition at Katherine, Australia. Cape Point, South Africa is essentially a maritime site and Torr de Paine, Chile is an inland site in the rain shadow of the Andes. If, based on the model's performance in the Northern Hemisphere, we accept that its long-range transport in the Southern Hemisphere is relatively realistic, we are left with three possible explanations for the background nitrogen: (1) explicit long-range transport of insoluble end-products such as PAN; (2) alternative local and regional sources of NO_y; (3) downward transport from the lower stratosphere and upper troposphere.

The current model does not explicitly allow for the long-range transport of an insoluble end-product such as PAN. Current observations find very little PAN in the maritime boundary layer of either hemisphere but as much as 0.1 ppbv over the North Pacific in the free troposphere. The only free troposphere measurements in the Southern Hemisphere are from a few flights over the South Atlantic between South America and Africa that find very little PAN (less than 0.01 ppbv) outside of local pollution (Rudolph et al., 1987). While a chemical scheme that allows for the formation of PAN should increase NO_y levels over the North Pacific, it is not clear, given a lifetime of 2 h at 20°C, 2 days at 0°C and 14 days at -10°C, that PAN will survive transport through the ITCZ and on to the South Pacific. However, we are developing a model with an explicit chemistry and three transported tracers (nitrogen oxides, HNO_3 and NO_3^-, PAN) to examine this possibility.

Unless there is a means to concentrate organic nitrogen in the surface layer of seawater, seasalt aerosol would not appear to be a major source. However, Prospero et al. (1985) and Savoie et al. (1988) have suggested lightning, long-range transport of emissions from biomass burning and stratospheric injection as possibilities. Lightning is very difficult to quantify and much more variable in space and time than the background NO_y. The long-range transport of nitrogen emissions from biomass burning in the tropics, most likely in the form of PAN, is a possibility, though there are no observations to support this transport.

Past calculations of downward transport from the stratosphere (Levy et al., 1980) explain approximately half of the background. An interesting point is the qualitative similarity between seasonal cycles at Samoa for surface

measurements of O_3 (Oltmans, 1981), which is known to be supplied from the stratosphere (Levy et al., 1985) and surface measurements of NO_y (Savoie et al., 1988). Measurements of NO_y and PAN in the free troposphere over the South Pacific would help identify transport from aloft, be it long-range transport of PAN from the northern mid-latitudes and tropical regions of biomass burning, or NO_y transported from the stratosphere and the upper troposphere.

4. Conclusions

Using a medium-resolution transport model with realistic meteorology, no explicit chemistry, and simple parameterized wet and dry deposition, we have simulated the contribution of NO_x emissions from fossil fuel combustion to the global NO_y climatology and we conclude the following.

(1) Asian emissions, which produce a springtime maximum from Shemya to Fanning, are the major source of NO_y in the North Pacific. In addition, there is summertime transport of NO_y from the US out into the central subtropical Pacific.

(2) European emissions are the dominant source of the nitrogen component of Arctic haze. A large longitudinal gradient (factor of 10 or more) is predicted with the minimum over Alaska and the maximum over northern Scandinavia and the Soviet Union.

(3) Almost none of the NO_y from fossil fuel combustion in the Northern Hemisphere is transported into the Southern Hemisphere. The little that is, as well as the prescribed Southern Hemisphere emissions, can explain no more than 10% of the background nitrogen that dominates both the nitrogen budget of the Southern Hemisphere and the NO_y climatology outside of continental source regions. While the long-range transport of PAN, local marine biogenic production, and lightning sources are all possible explanations, we predict that stratospheric injection is a major source of background NO_y in the Southern Hemisphere.

Measurements of individual reactive nitrogen species and total NO_y are needed throughout the free troposphere, particularly in the Southern Hemisphere where there are almost none.

Future model developments will include chemistry, transport of individual nitrogen compounds, PAN in particular, and a seasonal and surface dependent dry deposition parameterization.

5. Acknowledgements

We wish to thank Osten Hov, Sultan Hameed and Jane Dignon for providing emission data, Charles W. Black and Louisa A. Bogar for constructing the global emission field, Dennis Savoie and James Galloway for providing unpublished observations and Anton Eliassen, Douglas Whelpdale, Dennis Savoie and James Galloway for many helpful comments and discussion.

REFERENCES

Atlas, E. 1988. Evidence for $>C_3$ alkyl nitrates in rural and remote atmospheres. *Nature 331*, 426–438.

Barrie, L. A. 1986. Arctic air pollution: an overview of current knowledge. *Atmos. Environ. 20*, 643–663.

Barrie, L. A. and Hales, J. M. 1984. The spatial distributions of precipitation acidity and major ion wet deposition in North America during 1980. *Tellus 36B*, 333–355.

Barrie, L. A., Olson, M. P. and Oikawa, K. K. 1989. The flux of anthropogenic sulfur into the Arctic from mid-latitudes in 1979/80. *Atmos. Environ.*, in press.

Bottenheim, J. W., Gallant, A. G. and Brice, K. A. 1986. Measurements of NO_y species and O_3 at 82°N latitude. *Geophys. Res. Lett. 13*, 113–116.

Cadle, S. H., Dasch, J. M. and Mulawa, P. A. 1985. Atmospheric concentrations and the deposition velocity to snow of nitric acid, sulfur dioxide and various particulate species. *Atmos. Environ. 19*, 1819–1827.

Chang, J. S., Brost, R. A., Isaksen, I. S. A., Middleton, P., Stockwell, W. R. and Walcek, C. J. 1987. RADM, a three-dimensional Eulerian acid deposition model. Part I: Physical concepts and model formulation. *J. Geophys. Res. 92*, 14681–14700.

Crutzen, P. J. 1974. Photochemical reaction initiated by and influencing ozone in unpolluted tropospheric air. *Tellus 26*, 58–70.

Crutzen P. J., Delany, A. C. Greenberg, F., Haagenson, P., Heidt, L., Jueb, R., Pollock, W.,

Seiler, W., Wartburg, A. and Zimmerman, P. 1985. Tropospheric chemical composition measurements in Brazil during the dry season. *J. Atmos. Chem. 2*, 233–256.

Eliassen, A., Hov, O., Iversen, T., Saltbones, J. and Simpson, D. 1988. *Estimates of airborne transboundary transport of sulphur and nitrogen over Europe*. Oslo, Norway: The Norwegian Meteorological Institute Meteorological Synthesizing Centre, West, of EMEP.

Fahey, D. W., Hubler, G., Parrish, D. D., Williams, E. J., Norton, R. B. and Ridley, B. A. 1986. Reactive nitrogen species in the troposphere. *J. Geophys. Res. 91*, 9781–9793.

Fehsenfeld, F. C., Parrish, D. D. and Fahey, D. W. 1988. The measurement of NO_x in the non-urban troposphere. In *Tropospheric ozone* (ed. I. S. A. Isaksen). Dordrecht: D. Reidel Publishing Co., 185–215.

Galasyn, J. F., Tschudy, K. L. and Huebert, B. J. 1987. Seasonal and diurnal variability of nitric acid vapor and ionic aerosol species in the remote free troposphere at Mauna Loa, Hawaii. *J. Geophys. Res. 92*, 3105–3113.

Galloway, J. N. and Whelpdale, D. M. 1987. WATOX-86 overview and western North Atlantic Ocean S and N atmospheric budgets. *Global Biogeochem. Cycles 1*, 261–281.

Garland, J. A. and Penkett, S. A. 1976. Absorption of peroxy acetyl nitrate and ozone by natural surfaces. *Atmos. Environ. 10*, 1127–1131.

Golomb, D. 1983. Acid deposition–precursor emission relationship in the northeastern USA. The effectiveness of regional emission reduction. *Atmos. Environ. 17*, 1387–1390.

Hameed, S. and Dignon, J. 1988. Changes in the geographical distributions of global emissions of NO_x and SO_x from fossil-fuel combustion between 1966 and 1980. *Atmos. Environ. 22*, 441–449.

Huebert, B. J. and Robert, C. H. 1985. The dry deposition of nitric acid to grass. *J. Geophys. Res. 90*, 2085–2090.

Johansson, C. and Granat, L. 1986. AN experimental study of the dry deposition of gaseous nitric acid to snow. *Atmos. Environ. 20*, 1165–1170.

Leighton, P. A. 1961. *Photochemistry of Air Pollution*. New York: Academic Press, 300 pp.

Leone, J. A. and Seinfeld, J. H. 1985. Comparative analysis of chemical reaction mechanisms for photochemical smog. *Atmos. Environ. 19*, 437–464.

Levy II, H. 1971. Normal atmosphere: large radical and formaldehyde concentrations predicted. *Science 173*, 141–143.

Levy II, H., Mahlman, J. D. and Moxim, W. J. 1982. Tropospheric N_2O variability. *J. Geophys. Res. 87*, 3061–3080.

Levy II, H., Mahlman, J. D. and Moxim, W. J. 1980. A stratospheric source of reactive nitrogen in the unpolluted troposphere. *Geophys. Res. Lett. 7*, 441–444.

Levy II, H., Mahlman, J. D., Moxim, W. J. and Liu, S. C. 1985. Tropospheric ozone: the role of transport. *J. Geophys. Res. 90*, 3753–3772.

Levy II, H. and Moxim, W. J. 1987. The fate of US and Canadian combustion nitrogen emissions. *Nature 328*, 414–416.

Levy II, H. 1974. Photochemistry of the troposphere. In *Advances in Photochemistry, Vol. 9* (ed. J. N. Pitts, Jr., G. S. Hammond and K. Gollnick). New York: John Wiley and Sons, Inc., 369–524.

Liu, S. C., McAfee, J. R. and Cicerone, R. J. 1984. Radon 222 and tropospheric vertical transport. *J. Geophys. Res. 89*, 7291–7297.

Logan, J. 1983. Nitrogen oxides in the troposphere: global and regional budgets. *J. Geophys. Res. 88*, 10785–10807.

Mahlman, J. D. and Moxim, W. J. 1978. Tracer simulation using a global general circulation model: results from a midlatitude instantaneous source experiment. *J. Atmos. Sci. 35*, 1340–1374.

Manabe, S., Hahn, D. G. and Holloway, Jr., J. L. 1974. The seasonal variation of the tropical circulation as simulated by a global model of the atmosphere. *J. Atmos. Sci. 31*, 43–83.

Manabe, S. and Holloway, Jr., J. L. 1975. The seasonal variation of the hydrologic cycle as simulated by a global model of the atmosphere. *J. Geophys. Res. 80*, 1617–1649.

McFarland, M., Kley, D., Drummond, J. W., Schmeltekopf, A. L. and Winkler, R. H. 1979. Nitric oxide measurements in the equatorial Pacific region. *Geophys. Res. Lett. 6*, 605–608.

Merrill, J. T., Bleck, R. and Avila, L. 1985. Modeling atmospheric transport to the Marshall Islands. *J. Geophys. Res. 90*, 12927–12936.

Mitchell, M. 1956. Visual range in the polar regions with particular reference to the Alaskan Arctic. *J. Atmos. Terr. Phys. Special Supplement*, 195–211.

National Res. Council. 1983. *Acid deposition: atmospheric processes in Eastern North America, a Review of current scientific understanding*. Washingotn, D.C.: National Academy Press, 375 pp.

Oltmans, S. J. 1981. Surface ozone measurements in clean air. *J. Geophys. Res. 86*, 1174–1180.

Plumb, R. A. and Mahlman, J. D. 1987. The zonally averaged transport characteristics of the GFDL general circulation/transport model. *J. Atmos. Sci. 44*, 298–327.

Prather, M. J., McElroy, M., Wofsy, S., Russell, G. and Rind, D. 1987. Chemistry of the global troposphere: fluorocarbons as tracers of air motion. *J. Geophys. Res. 92*, 6579–6613.

Prospero, J. M., Savoie, D. L., Nees, R. T., Duce, R. A. and Merrill, J. 1985. Particulate sulfate and nitrate in the boundary layer over the North Pacific Ocean. *J. Geophys. Res. 90*, 10586–10596.

Rahn, K. A., Borys, R. D. and Shaw, G. E. 1977. The Asian source of Arctic haze bands. *Nature 268*, 713–715.

Rudolph, J., Vierkorn-Rudolph, B. and Meixner, F. X. 1987. Large-scale distribution of peroxyacetylnitrate results from the STRATOZ III flights. *J. Geophys. Res. 92*, 6653–6661.

Savoie, D. L., Prospero, J. M. and Graustein, W. C. 1988. Background concentrations of nitrate in the marine boundary layer (Abstract). *Eos Trans. AGU 69*, 317.

Schaug, J., Hansen, J. E., Nodop, K., Ottar, B. and Pacyna, J. M. 1987. *Summary Report from the Chemical Co-ordinating Centre for the Third Phase of EMEP.* Lillestrom, Norway: Norwegian Institute for Air Research.

Singh, H. B., Salas, L. J. and Viezee, W. 1986. The global distribution of peroxyacetyl nitrate. *Nature 321*, 588–591.

Stockwell, W. R. 1986. A homogeneous gas phase mechanism for use in a regional acid deposition model. *Atmos. Environ. 20*, 1615–1632.

Summers, P. W. and Barrie, L. A. 1986. The spatial and temporal variation of the sulfate to nitrate ratio in eastern North America. *Water, Air, and Soil Pollution 30*, 275–283.

Trainer, M., Williams, E. J., Parrish, D. D., Buhr, M. P., Allwine, E. J., Westberg, H. H., Fehsenfeld, F. C. and Liu, S. C. 1987. Models and observations of the impact of natural hydrocarbons on rural ozone. *Nature 329*, 705–707.

Uematsu, M., Duce, R. A., Prospero, J. M., Chen, L. Q., Merrill, J. T. and McDonald, R. L. 1983. The transport of mineral aerosol from Asia over the North Pacific Ocean. *J. Geophys. Res. 88*, 5343–5352.

Voldner, E. C., Barrie, L. A. and Sirois, A. 1986. A literature review of dry deposition of oxides of sulfur and nitrogen with emphasis on long-range transport modelling in North America. *Atmos. Environ. 20*, 2101–2123.

Walcek, C. J., Brost, R. A., Chang, J. S. and Wesely, M. L. 1986. SO_2, sulfate, and HNO_3 deposition velocities computed using regional land use and meteorological data. *Atmos. Environ. 20*, 949–964.

Wesely M. L., Eastman, J. A., Stedman, D. H. and Yalvac, E. D. 1982. An eddy correlation measurement of NO_2. *Atmos. Environ. 16*, 815–820.